Geophys. J. R. astr. Soc. (1987) **88**, 25–41

Shear-wave splitting in the upper-mantle wedge above the Tonga subduction zone

J. Roger Bowman* *Cooperative Institute for Research in Environmental Sciences, Campus Box 449, University of Colorado, Boulder, CO 80309, USA*

Masataka Ando *Disaster Prevention Research Institute, Uji, Kyoto 611, Japan*

Accepted 1986 March 15. Received 1986 March 10; in original form 1985 April 14

Summary. Intermediate-period seismograms of shear waves from deep earthquakes are examined for shear-wave splitting diagnostic of seismic velocity anisotropy in the upper-mantle wedge between the subducting Tonga slab and stations in the Fiji Islands. Earthquakes with near-vertical incidence angles are selected to minimize complications of converted phases and the free surface. Horizontal-component seismograms for 25 deep earthquakes recorded at station LAK on the Lau Ridge show splitting of up to 0.9 s with an average of 0.45 ± 0.25 s between fast and slow *S*-wave components. Anisotropy in the upper mantle is the most likely cause of the splitting. The ESE orientation of the fast velocity direction at station LAK corresponds to an axis of symmetry of the anisotropic mantle and is approximately perpendicular to magnetic lineations in the Lau Basin and the northeastern portion of the South Fiji Basin. The observations are consistent with a model of flow alignment of olivine (100) and orthopyroxene (001) axes parallel to the direction of basin extension. Seismograms for eight deep earthquakes at station SVA on Viti Levu show up to 1.0 s splitting with an average of 0.65 ± 0.29 s and a weak NNE preferred orientation of fast velocity. Polarizations of shear-wave particle motions corrected for anisotropy are within 36° ± 26° of polarizations predicted for nine moment tensor solutions. The magnitude of shear-wave splitting and estimates of the thickness of the lithosphere in the Fiji region imply that the anisotropy cannot be contained in the lithosphere alone. Either the anisotropy is distributed in both the lithosphere and asthenosphere, or the asthenosphere alone is anisotropic.

Key words: shear waves, seismic anisotropy, upper mantle, subduction zone

* Now at: Research School of Earth Sciences, Australian National University, GPO Box 4, Canberra, ACT 2601, Australia.

Introduction

Although seismologists widely assume that the earth is isotropic, evidence is mounting that the mantle is anisotropic and that velocity anistropy must be considered in order to model mantle structure adequately. The first observations of anisotropy were of the azimuthal variation of P_n velocities derived from refraction data (e.g. Hess 1964). Anisotropy has also been suggested to explain the discrepancy between oceanic velocity structures derived from Love and Rayleigh waves (Forsyth 1975) and was included as a parameter in the global inversion of surface and body wave data PREM (Dziewonski & Anderson 1981). Measurement of velocity anisotropy in the mantle may help detect tectonic deformation and reveal dynamic processes in the mantle. For example, the fast direction of P_n is interpreted to coincide with the spreading direction at the time and site of formation of shallow mantle material (e.g. Hess 1964; Raitt *et al.* 1971). Observations of anisotropy from ScS waves (Ando 1984) and surface waves (Tanimoto & Anderson, 1984) show agreement between the azimuth of fast *S*-wave components or Rayleigh waves and the direction of flow expected from plate tectonic considerations.

A difficult problem is encountered in measuring seismic velocity anisotropy by using earthquake sources and receivers with ray paths over a wide range of azimuths. Even if appropriate sources and receivers are found, questions of lateral inhomogeneity and source variability can complicate interpretations of anisotropy. An alternate approach which avoids this problem is to examine the two orthogonally polarized *S*-wave components that traverse nearly identical paths. Synthetic seismograms show that readily observable features of seismic body-wave propagation in anisotropic media are the polarization anomalies caused by shear-wave splitting (e.g. Keith & Crampin 1977). These polarization anomalies are seen in particle motion diagrams as departures from the direction of particle motion predicted by isotropic theory. Since the polarized shear waves arrive at different times, the particle motion is not rectilinear and is thus unlike that of waves which have travelled through an isotropic medium. Shear-wave splitting and resultant polarization anomalies are diagnostic of anistropic propagation, and can be used to estimate the symmetry and degree of anistropy in a volume.

The Fiji and Tonga Islands region is an ideal place to study upper-mantle anisotropy for several reasons. In that region the Pacific plate is subducting beneath the Australia–India plate (Oliver & Isacks 1967). The geometry of subduction is fairly simple and well-studied (Sykes, Isacks & Oliver 1969; Billington 1980). A large portion of the world's deep earthquakes occur in the subducted slab in the Fiji deep seismic zone, and islands are located close to the deep earthquake epicentres, which allows recording in the shear-wave window. Deep events in the area can generally be modelled by simple source time functions (Pennington & Isacks 1979).

Data

Three-component, portable digital seismographs were installed at two sites over the deep seismic zone in Fiji in 1983 July and operated intermittently through 1985 May. One of these stations (SVA) was located on Viti Levu, the largest island of the Fiji group, and the other (LAK) was on the island of Lakeba on the Lau Ridge (Fig. 1). The Lau Ridge is a remnant arc which was rafted away from the Tonga Ridge about 6 Ma by the opening of the Lau Basin by back-arc spreading (Karig 1970; Weissel 1977). Viti Levu and Vanua Levu are on an extension of the Lau Ridge (Gill & Gorton 1973), which has been rotated counterclockwise by about 90° in the past 7 Myr (Malahoff *et al.* 1982a). Thus, both seismograph

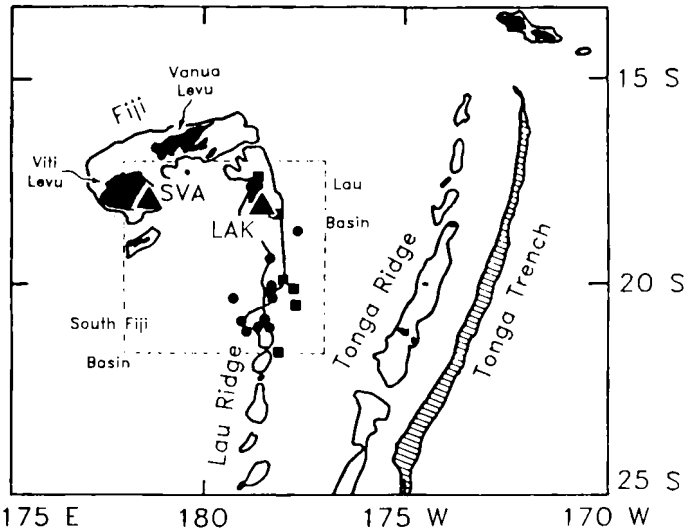

Figure 1. Generalized bathymetric map of the southwest Pacific with contours for 1000 m (open) and 7500 m (cross-hatched) from Kroenke, Jouannic & Woodward (1983). Seismographs (triangles) and earthquakes between 425 and 550 km (squares) and deeper than 550 km (circles) used in this study are shown. Symbols for eight earthquakes are obscured by LAK station symbol. Dashed box shows map area of Fig. 6.

sites are on an inactive island arc structure. These seismographs provided the first digital data for the Fiji region, and intermediate-period seismometers provided broader-band response to ground motion than was previously available. The horizontal-component seismometers had natural periods of 5 s, and the vertical-component seismometers, of 2 s. Data were sampled at 50 Hz. Station LAK was the first seismograph deployed on the Lau Ridge for more than a brief period. Very few shallow, local earthquakes were recorded at LAK. During 18 months of event-triggered recording, the two closest earthquakes had $S-P$ times of 7 and 8 s and only three others had $S-P$ times of less than 15 s.

The seismograph system was configured for recording deep earthquakes of moderate magnitude (m_b 4.5–6.0). Although the intermediate-period seismometers passed microseismic noise, they had the advantage of not attenuating the low-frequency component of waveforms from deep earthquakes. Amplifier gains of only 54–60 db were sufficient to provide full-scale recording for earthquakes of m_b 5.5–6.0. The seismographs were event recorders, and recording was triggered by the signal from a single seismometer. In the first year of data collection, the signal from a horizontal seismometer was used for the trigger to ensure recording of the S-phase. Since the horizontal component of the P-wave for deep earthquakes with near-vertical angles of incidence is small, some earthquakes did not trigger the seismograph until the S-wave arrival. Later in the study, the trigger was changed to the vertical component in an attempt to record both the P- and S-waves.

Earthquakes selected for this study were deeper than 425 km, within 4° of each recording station, and had S-wave signal-to-noise ratios greater than four. Twenty-five earthquakes at station LAK and eight at SVA met these criteria (Table 1, Fig. 1). Hypocentres for the events studied were found in the Preliminary Determination of Epicentres (PDE). Three earthquakes in this group were well-recorded at both stations.

Some features of the data are illustrated by seismograms of earthquake no. 16 which was

Table 1. Deep earthquakes used for this study.*

event #	yr	mon	day	time	latitude (°S)	longitude (°W)	depth (km)	m_b
1	83	07	17	06:29:18.9	18.539	177.660	586	5.2
2	83	08	03	22:41:03.3	19.862	178.346	614	5.2
3	83	08	14	16:20:12.2	17.221	178.697	516	5.0
4	83	08	27	04:14:27.4	20.826	178.682	618	4.8
5	83	09	10	12:51:40.1	17.968	178.447	639	4.7
6	83	10	21	17:04:07.6	18.035	178.526	607	4.9
7	83	11	23	05:48:33.5	18.105	178.333	607	5.6
8	83	11	30	16:40:45.8	17.955	178.500	591	4.9
9	83	12	08	02:19:10.9	19.216	178.378	627	5.5
10	83	12	24	18:21:50.7	20.144	178.319	599	5.4
11	83	12	27	20:45:41.8	19.942	177.796	426	4.7
12	84	01	20	03:53:02.8	17.833	178.571	534	5.2
13	84	01	29	08:27:38.6	20.318	177.735	526	4.5
14	84	06	25	16:58:16.4	18.091	178.684	567	4.7
15	84	06	30	12:10:10.1	17.774	178.767	571	4.8
16	84	07	03	13:42:00.8	17.735	178.847	536	5.7
17	84	07	03	13:47:06.4	17.651	178.876	530	5.2
18	84	07	11	06:23:20.4	21.441	178.229	472	5.2
19	84	07	20	13:55:40.1	20.850	178.410	574	5.2
20	84	08	21	12:17:57.7	18.025	178.457	607	4.9
21	84	08	22	05:18:41.5	20.023	178.425	616	5.2
22	84	08	23	07:15:55.5	19.756	178.068	440	4.9
23	84	09	01	21:16:12.8	18.197	178.168	478	5.4
24	84	10	10	19:05:57.8	20.158	179.339	674	5.6
25	84	10	20	21:22:11.3	20.645	178.510	575	5.4
26	84	10	22	16:51:19.4	17.682	178.739	594	4.6
27	84	12	24	21:04:59.8	17.455	178.874	558	4.7
28	85	01	09	01:32:38.9	20.754	179.085	662	5.3
29	85	04	02	03:21:41.4	21.236	179.075	636	5.4
30	85	05	16	01:06:18.6	17.786	178.633	577	5.2

* Hypocenters from monthly *PDE*.

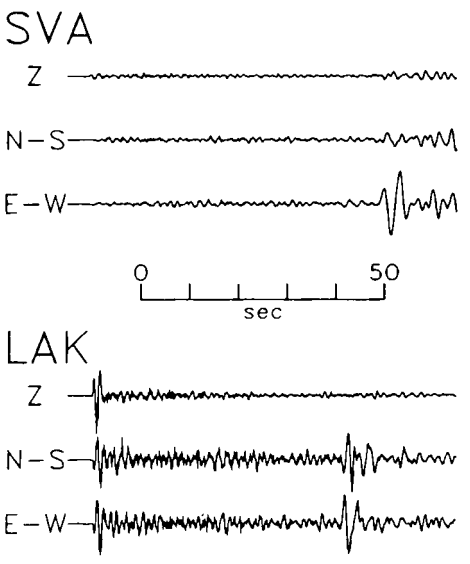

Figure 2. Sample seismograms from earthquakes no. 16 recorded at stations SVA and LAK. Location of event no. 16 is shown in Fig. 6. *P*-arrival is nodal at SVA. Vertical and horizontal seismometers have natural periods of 2 and 5 s respectively. Horizontal-component gain is 1.5 times vertical.

located at a depth of 536 km and recorded at both stations (Fig. 2). The *S* amplitude on the horizontal components is large relative to the amplitude on the vertical components, and the *S*-signal to *P*-coda (noise) ratio is high. *S*–*P* times of 50 s at LAK and 60 s at SVA are typical for earthquakes 500 to 600 km deep. Generally, the signal-to-noise ratio for the *S*-phase was higher at LAK than SVA; in some cases the *S*-amplitude did not exceed the *P*-coda level at SVA. Several additional characteristics of the *S*-wave data are notable. Occasional long-duration *S*-phases with numerous oscillations were interpreted as resulting from complex sources and were not used for this study. Several earthquakes consisted of two discrete events separated by about 5 s in the *P*-wave on the vertical component and the *S* on the horizontal (nos 22 and 23). The two horizontal components for some earthquakes are quite different in form (event nos 2, 4, 8, 21 and 28). On one component the *S*-wave looks like a simple pulse, while on the other component the *S*-wave is more complex with an extra pulse superimposed on the initial *S*-phase. Earthquakes exhibiting this extra pulse were concentrated between 19.5° and 20.5° *S* and deeper than 600 km suggesting that multi-pathing through the slab or anisotropy in the slab may produce the extra phase on one component.

Analysis of shear-wave particle motions

The orientation and magnitude of shear-wave splitting in an anisotropic medium depend on the orientation of the ray relative to the symmetry axes as well as the elastic constants and density of the medium. We do not know *a priori* either the symmetry class or orientation of symmetry axes relative to the Earth. Because the deep earthquakes studied here have small angles of incidence at the free surface, most of the shear-wave motion is in the horizontal

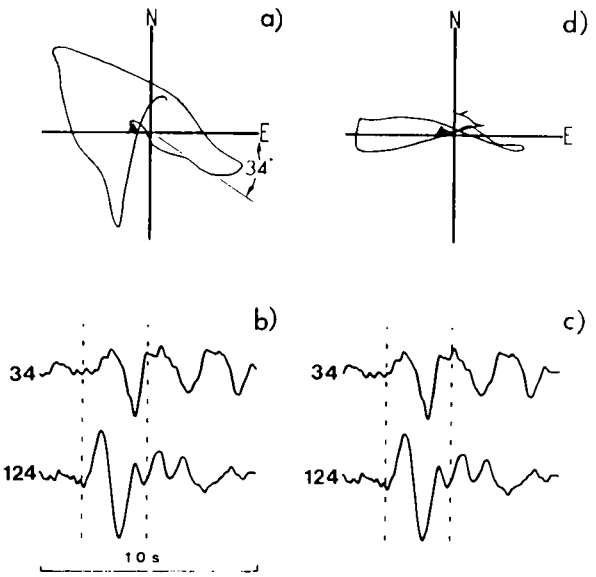

Figure 3. Example of data analysis procedure for earthquake no. 16: (a) original horizontal particle motion, (b) seismograms rotated by angle determined in (a), (c) rotated seismograms with upper trace advanced by 0.54 s, the time shift which gives maximum absolute value of cross-correlation coefficient between traces, (d) particle motion corrected for anisotropy. Dashed lines show section of seismogram for which particle motion is plotted. Triangles show start of particle motion.

plane (see Fig. 2), and we restrict the present analysis to the horizontal components. The N–S and E–W components of ground motion which were recorded in this study are not necessarily parallel to the principal axes of anisotropy, and shear-wave splitting in other than the recorded directions may be masked by mixing the split components of the shear wave on the two recorded traces. Therefore, the first objective of the analysis is to find a coordinate rotation that best resolves the orthogonal *S*-wave components.

Two methods were used to evaluate shear-wave splitting. The first method is illustrated for event no. 16 recorded at station LAK in Fig. 3. The orientation of the first *S* motion was measured from a plot of the horizontal particle motion of the *S*-wave (Fig. 3a). The seismograms were rotated by the measured angle (Fig. 3b), and the cross-correlation coefficient between the rotated traces was computed for time lags of +2 to −2 s. The time lag that produced the maximum or minimum correlation coefficient was considered a measure of the splitting between the two shear waves. The slower component was then advanced relative to the faster component by the appropriate time lag (Fig. 3c), the data were re-rotated to a N–S coordinate system and the 'corrected' particle motion was plotted (Fig. 3d). Visual comparison of the shifted traces and the linearity of corrected particle motion supplemented the cross correlation in determining the most appropriate time shift. Notice that the corrected particle motion is significantly more linear than the original. Another example of the analysis is shown in Fig. 4.

In the second method, a more quantitative approach was used to determine the orientation and splitting. The seismograms for each earthquake were rotated from 0° to 90° at 5° intervals, and the maximum and minimum cross-correlation coefficients were found for time lags of +1 to −1 s at each orientation. A plot of the maximum and minimum coefficients at each angle of rotation (Fig. 5) provides an idea of the 'correlation space' between the components of horizontal ground motion. The angle (or angles) of rotation resulting in the maximum amplitude value of correlation was then used in lieu of the observed first motion direction of the first method as the orientation which best resolved

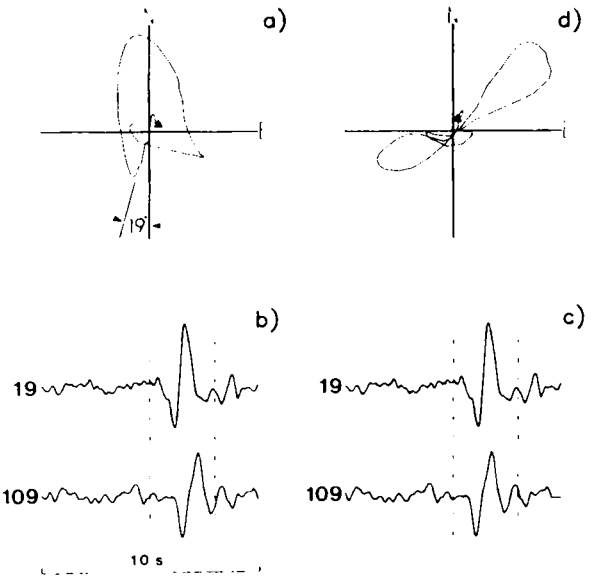

Figure 4. Analysis procedure for event no. 15. In (c) the lower trace is advanced by 0.45 s relative to the upper trace. Other details as in Fig. 3.

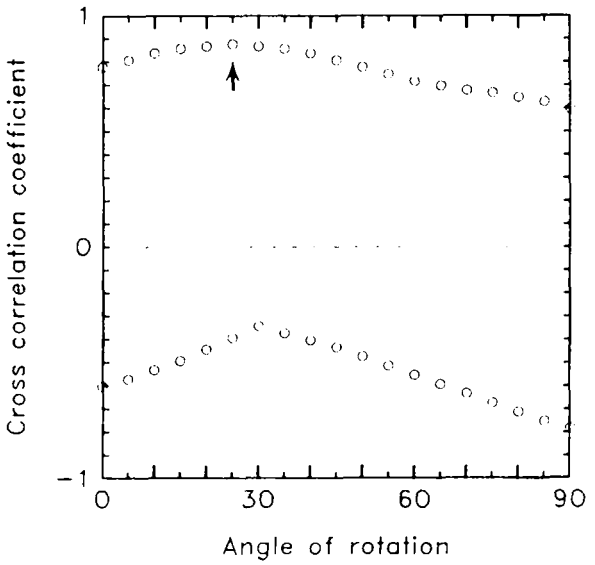

Figure 5. Maximum and minimum cross-correlation coefficients between rotated horizontal component of *S*-wave of event no. 16 recorded at station LAK. Time lag ranged from +1 to −1 s. Arrow shows angle of rotation giving best cross correlation.

the shear-wave splitting. For earthquake no. 16, for example, a rotation of 25° produced the maximum cross-correlation coefficient (Fig. 5). Subsequent steps of the analysis were the same as in the first method. In most cases the two methods produced essentially the same result. For event no. 16, the two results were within 10° and 0.1 s, and the result of the second method was used. When they disagreed, the result which produced the simplest particle motion and best aligned the *S*-wave onsets on the rotated, time-shifted seismograms was used for the following interpretation.

Observations of shear-wave splitting

Most deep earthquakes recorded in this study had non-rectlinear shear-wave polarization. This polarization was examined to determine the rotation and time shift which could correct for the anomalous polarization. The orientation of the fast *S*-wave component and the magnitudes of *S* splitting at stations LAK and SVA are shown in Fig. 6 and tabulated in Table 2. Quality factors were assigned to each splitting estimated based on signal-to-noise level and uniqueness of the estimate. Quality A and B earthquakes are plotted as dark lines in Fig. 6 and quality C, as light lines. Earthquakes with splitting of less than 0.1 s were considered to have linear polarization, and the original polarization directions are plotted as dashed lines in Fig. 6. Although the splitting vector is plotted at the earthquake epicentre, this does not imply that the cause of the splitting is at the earthquake source.

A clear pattern of shear-wave splitting is evident at station LAK (Fig. 6a). The distribution of splitting vectors determined for LAK is summarized in an azimuthal diagram in Fig. 6(a), where the orientation of each line shows the orientation of the fast *S*-wave component, and the length is proportional to the time difference between the two *S*-wave components. This presentation shows the largest splitting vectors to have a SE orientation, with the majority of observations distributed from NE to SE and four directed nearly N–S.

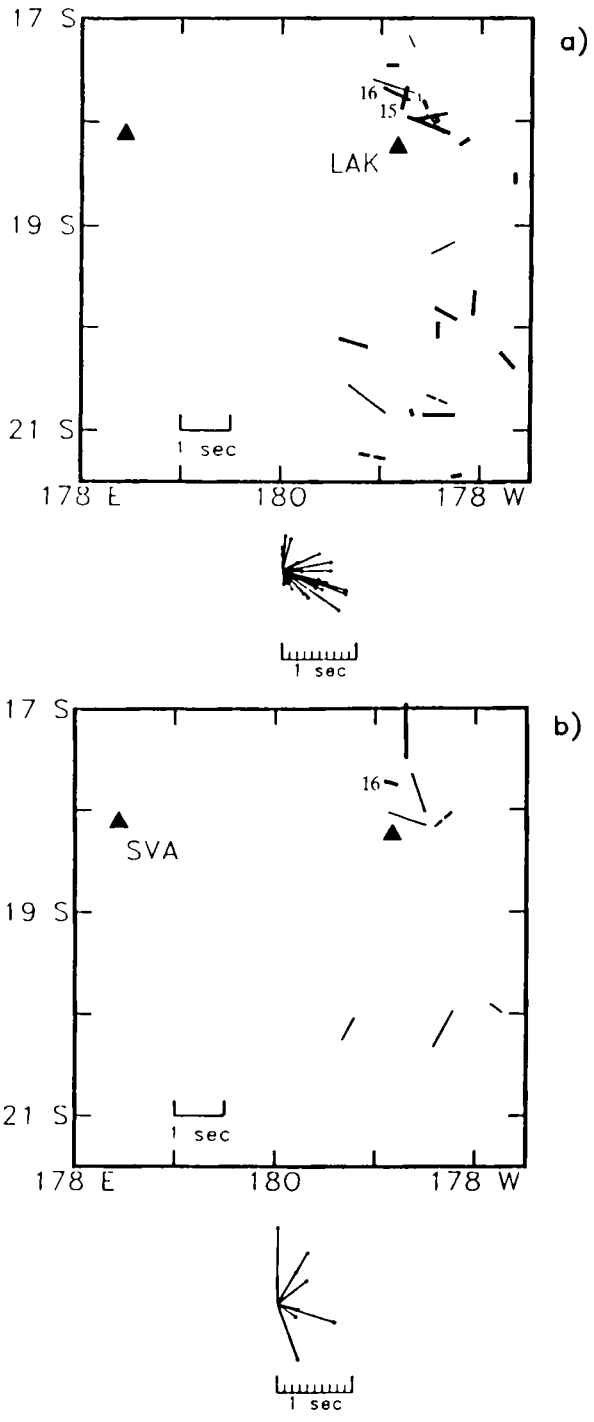

Figure 6. Map showing fast *S*-wave direction for earthquakes recorded at station (a) LAK and (b) SVA. Vector lengths are proportional to the time shift between split *S*-wave components. Heavy lines are for quality A and B data, and light lines for quality C. Dashed lines show orientation of linear particle motion with arbitrary length. Each vector is centred on epicentre of earthquake. Diagrams of vectors showing direction and magnitude of shearwave splitting in horizontal plane are shown to the right of each map.

Table 2. Shear-wave splitting.

	SVA					LAK				
Event #	Δ	Φ	Θ	Δt	Q,C	Δ	Φ	Θ	Δt	Q,C
1	--	--	--	--	--	1.2	10	0	0.22	A
2	--	--	--	--	--	1.7	13	117	0.50	B
3	2.9	25	0	1.04	B	1.0	10	153	0.32	C,2
4	--	--	--	--	--	2.6	19	155	0.14	B,2
5	--	--	--	--	--	0.4	3	150	0.18	B
6	--	--	--	--	--	0.3	3	110	0.91	A
7	3.1	23	25 (51)	0.06	B,5	--	--	--	--	--
8	--	--	--	--	--	0.4	4	80	0.66	B,2
9	--	--	--	--	--	1.1	8	65	0.54	C,3
10	3.7	26	30	0.80	C	--	--	--	--	--
11	4.0	37	125	0.30	C	--	--	--	--	--
12	2.9	24	160	0.80	C	--	--	--	--	--
13	--	--	--	--	--	2.3	21	137	0.42	A
14	2.7	22	108	0.80	C	--	--	--	--	--
15	--	--	--	--	--	0.5	4	15	0.45	A
16	2.6	22	104	0.28	A	0.5	5	115	0.59	A
17	--	--	--	--	--	0.6	6	107	0.90	C,2
18	--	--	--	--	--	3.3	30	80	0.21	A
19	--	--	--	--	--	2.6	21	90	0.65	B
20	--	--	--	--	--	0.4	3	90 (136)	0.07	C,4
21	--	--	--	--	--	1.8	14	0	0.32	A,2
22	--	--	--	--	--	1.7	19	5	0.48	B
23	--	--	--	--	--	0.6	7	60	0.23	B,1
24	2.9	20	30	0.50	C	2.0	14	105	0.61	A
25	--	--	--	--	--	2.4	20	155 (111)	0.03	A,4
26	--	--	--	--	--	0.6	5	155	0.18	A
27	--	--	--	--	--	0.8	7	90	0.26	B
28	--	--	--	--	--	2.5	17	125	0.93	C,2
29	--	--	--	--	--	2.9	20	152 (102)	0.08	B,2,4
30	--	--	--	--	--	1.0	8	173	0.16	C,2

Δ Distance to hypocenter
Φ Incidence angle at surface
Θ Azimuth of fast S-wave component
Δt Time difference between S-wave
( ) Numbers in brackets are orientation of linear particle motion

Q,C Quality of S-wave splitting estimate, comments
1. Multiple event
2. Dissimilar waveforms on
3. Clipped seismograms
4. Linear particle motion

The same data are presented in a histogram of the number of events with fast *S*-waves at different azimuths in Fig. 7. Quality A observations are shaded. The semi-circular vector mean (Pincus 1956) direction of the splitting vectors is N123°E. The smooth curve shows the semi-circular normal distribution predicted for the vector mean and the variance of these data (e.g. Agterberg 1974, p. 480), while the horizontal dashed line shows the probability for a uniform distribution. The semi-circular normal distribution appears to give a better fit to the observations than a uniform distribution, although there are too few data to evaluate their significance with a chi-squared test. We will interpret the results based on ESE mean fast *S*-wave direction and discuss sources of scatter in the splitting data later. Linear polarizations of three earthquakes (nos 20, 25 and 29) have a trend similar to the fast *S*-wave direction (the dashed line for event no. 20 is obscured by splitting vectors east of LAK). For 22 earthquakes with non-linear horizontal particle motion, the fast *S*-wave arrives 0.45 ± 0.25 s before the orthogonal component with a maximum splitting of 0.93 s. This is less than

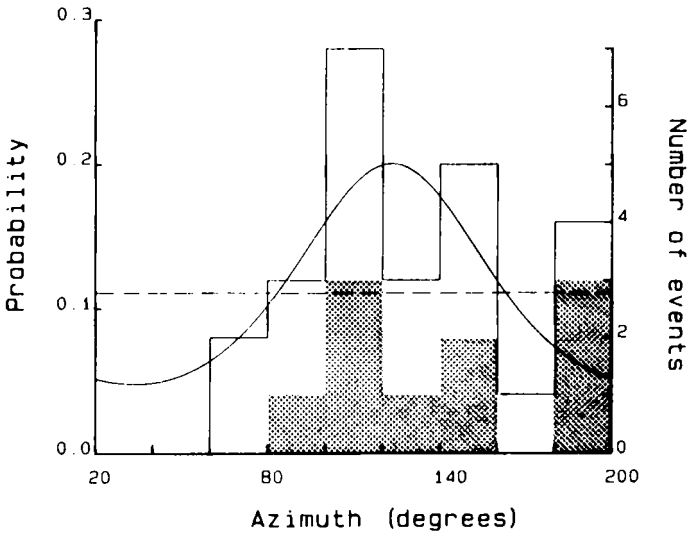

Figure 7. Histogram of number of earthquakes with shear-wave splitting in azimuth intervals observed at LAK. Shaded area shows quality A observations. Solid curve is semi-circular normal probability distribution. Dashed line shows uniform probability.

the splitting of *S*-waves observed by Ando, Ishikawa & Yamazaki (1983) (~0.65 s) or the splitting of *ScS* waves observed by Fukao (1984) (~0.8 s) or Ando (1984) (~1.05 s).

Although there are fewer shear-wave splitting observations at station SVA, a pattern different from that at LAK emerges in Fig. 6(b). The shear waves at SVA are split by 0.65 ± 0.29 s, and the dominant fast direction, if it can be estimated from so few data, is closer to NNE than to the ESE orientation observed at LAK.

Two earthquakes recorded at both stations show different orientations of fast *S*-wave components at the two sites. Event no. 3 had a fast direction of 25° and a splitting of 1.0 s at SVA and 153° and 0.3 s at LAK. Event no. 24 had a fast direction of 30° and splitting of 0.5 s at SVA and 105° and 0.6 s at LAK. This implies that the fast *S*-wave direction reflects the propagation path rather than the source mechanism. On the other hand, event no. 16 had similar splitting with a fast direction of 104° and 115° and splitting of 0.3 and 0.6 s at SVA and LAK respectively.

Possible causes of polarization anomalies

A possible cause for the polarization anomalies observed in Fiji is seismic velocity anisotropy along the propagation path (Keith & Crampin 1977; Ando *et al.* 1983; Ando 1984; Cormier 1984). The delays between split arrivals and azimuthal variations of *S*-velocities are characteristic of various systems of anisotropy (e.g., Kasahara *et al.* 1968; Musgrave 1970). However, before concluding that elastic anisotropy is responsible for the polarization anomalies, it is prudent to consider the expected effects on horizontal particle motion caused by the free surface and possible converted phases. Shear-wave polarization can be severely distorted by the free-surface at angles of incidence greater than the critical angle for *S*-to-*P* conversion (~35°) (Nuttli 1961; Mendiguren 1969; Evans 1984). The present experiment was designed to study near-vertically incident ray paths from deep earthquakes in order to minimize free-surface and phase conversion effects. Stations were deployed

within 4° of deep earthquake sources. The angle of incidence at the free surface calculated for velocity model TNA (Grand & Helmberger 1984) for each earthquake studied is given in Table 2. All but one of these events (no. 11) had angles of incidence at least several degrees less than critical and were in the shear-wave window. For those earthquakes which had both *P*- and *S*-waves recorded, the apparent angle of incidence was measured directly from the *P*-wave particle motion in the vertical–radial plane, and the true angle calculated. The maximum observed angle of incidence was 17°, confirming that shear-wave polarization should not be distorted by the free surface.

S-to-*P* and *P*-to-*S* conversions at the Moho and shallower discontinuities can produce significant precursors to the *S*-phase (Kanasewich *et al.* 1973), which would contaminate the *S*-phase and contribute to polarization anomalies. For small angles of incidence, amplitudes of *S*-to-*P* converted phases would be significantly larger on the vertical than horizontal components (Kanasewich, Alpaslan & Hron 1973). However, none of the data used in this study showed a significant precursor or large primary *S*-phase on the vertical component. In fact the *S*-amplitude on the horizontal component was three to four times that of the vertical. *P*-to-*S* conversion at the slab–asthenosphere interface is another possible source of polarization anomalies. A *P*-to-*S* converted phase for an earthquake 15 km from the interface would arrive about 2.5 s before the direct *S*, which is a larger separation than observed in the data. Angles of incidence at the interface required for the direct *S* and *P*-to-*S* conversions were calculated for the geometry of this experiment, assuming the hypocentres to be 15 km inside the slab. The direct *S*-wave would have an angle of incidence of about 50° at the interface, whereas the *P*-to-*S* conversion would have an angle of incidence of almost 90°. The relative transmission coefficients for these phases indicate that the converted phase would have a very small amplitude relative to the direct phase. We conclude, therefore, that converted phases are not the primary source of the polarization anomalies observed at LAK and SVA.

Shear-wave polarizations predicted from earthquake source mechanisms provide a check on the anisotropy correction of the horizontal particle motion. Nine of the earthquakes used in this study have moment tensor solutions published in the monthly PDE report. Polarizations predicted from the moment tensor solutions were compared to the polarizations corrected for anisotropy for these events. The polarizations of the shear-wave particle motions that have been corrected for anisotropy agree with the predicted polarizations to within $36° \pm 26°$. The maximum difference is 76°. In general the polarizations agree well for moment tensors well fit by a double-couple mechanism, while the disagreement is larger for those events with a large non-double couple component. This suggests that the disagreement between the predicted and correct polarizations may be the result of poor constraint of the focal mechanism as well as error in estimating the take-off angles and applying the anisotropy correction. However, the polarization predicted for event no. 16, which had a moment tensor well fit by a double-couple solution, disagreed with the corrected polarization by 75°. For two events with no dominant polarization in the original horizontal particle motion, the corrected polarizations differed from those predicted by 24° and 34°. The reasonable agreement of the shear-wave polarizations corrected for anisotropy with the polarizations predicted from moment tensor solutions supports the interpretation of anisotropy as the cause of the observed shear-wave polarization anomalies.

One model suggested for producing regional-scale anisotropy in the upper mantle is flow alignment of olivine (e.g. Hess 1964; Christensen & Salisbury 1979) and orthopyroxene (Christensen & Lundquist 1982; Estey, Douglas & Spetzler 1986). Because olivine and orthopyroxene are intrinsically anisotropic, preferred crystallographic alignment of these minerals produces bulk anisotropy. Comparison of orientation of these minerals to the

mapped attitudes of the Moho and sheeted dikes in ophiolites indicates that flow produces an orthohombic fabric with olivine [100] and orthopyroxene [001] axes aligned in the flow direction, and the olivine [010] and orthopyroxene [100] axes aligned normal to the flow plane (Pesselnick & Nicolas 1978; Christensen 1984).

Observations of anisotropy elsewhere provide some preliminary constraints on the distribution of anisotropy in the Fiji–Tonga area. An abundance of P_n observations (e.g. Raitt *et al.* 1971; see Christensen 1984, for a compilation) and petrofabric analyses (e.g. Pesselnick & Nicolas 1978; Christensen 1984) require an anisotropic uppermost oceanic mantle. Explosion and earthquake apparent velocity measurements in the NW Pacific require anisotropy throughout the lithosphere (Shimamura 1984). Furthermore, it is reasonable to believe that anisotropy developed by flow alignment in the asthenosphere would be frozen into the lithosphere as it cools and thickens (Estey & Douglas 1986). A strongly anisotropic lithosphere is not inferred in some surface-wave studies (Schule & Knopoff 1977; Reagan & Anderson 1984), but it is in others (Kawasaki 1986). Surface-wave (Schule & Knopoff 1977; Reagan & Anderson 1984; Kawasaki 1986) and whole-Earth (Dziewonski & Anderson 1981) velocity inversions imply significant anisotropy in the asthenosphere to a depth of 220 km. The lack of anisotropy observed from surface waves below 220 km may reflect both a lack of resolution and a change from peridotite-like to eclogite-like composition (Anderson 1979, 1984; Estey & Douglas 1986). This compositional change would reduce the olivine content below 220 km, and the clinopyroxene- and garnet-rich piclogite would produce only half the shear-wave anisotropy of the peridotite above 220 km (Estey & Douglas 1986).

Distribution and orientation of anisotropy

The shear-wave splitting reported above can be used to constrain the distribution and orientation of anisotropic symmetry axes, and to infer flow directions in the upper mantle in the Fiji–Tonga region. We will concentrate on the splitting at LAK because there are more data to constrain the interpretation. Ray paths of earthquakes with split shear waves at LAK sample a 100 km by 200 km section of the mantle at depths of 220 km and shallower where anisotropy is most significant. Transverse isotropy has a single axis of symmetry, usually taken to be vertical. This produces no azimuthal variation of *P*- or *S*-wave velocities and thus could not produce the observed shear-wave splitting. We therefore look for a model of orthorhombic symmetry which satisfies the splitting data. It is assumed that one axis of symmetry is vertical and two are horizontal.

The ESE fast *S*-wave direction at LAK reflects the direction of an axis of symmetry of the anisotropic mantle. This interpretation is supported by three earthquakes (nos 20, 25, and 29) with linear shear-wave particle motions at LAK. The rectilinear particle motion implies either that rays from those earthquakes have propagated through an isotropic medium or that the polarization of the shear waves radiated from the sources is parallel to one of the axes of symmetry of an anisotropic medium. The observed shear-wave polarization for the only earthquake with a well-constrained moment tensor solution (event no. 25, N111°E) is within 6° of that predicted for the moment tensor solution (N117°E). The orientations of the linear partical motions agree well with the fast velocity direction (Fig. 6a), and we take this as support for the east–southeast direction as an axis of symmetry of the anisotropic mantle. The third axis is parallel to the slow *S*-wave direction, NNE.

An estimate of the minimum thickness of an anisotropic layer in the upper mantle can be made by considering extremes of composition and alignment in the mantle. The minimum

Table 3. Minimum thickness of anisotropic layer.

Vertical axis olivine	Vertical axis pyroxine	Single crystal olivine* (km)	Fully oriented pyrolite-piclogite (km)	50 per cent oriented pyrolite-piclogite
[100]	[001]	94	210	420
[010]	[100]	30	35	70
[001]	[010]	22	30	60

* Shear-wave velocities for olivine at room temperature and pressure are from Verma (1960).

thickness of the anisotropic layer which could produce the shear-wave splitting observed at LAK for the three possible orientations of three mantle models are given in Table 3. The orientation is defined by the choice of the vertical axis of olivine. The corresponding orthopyroxene axes from crystallographic relations in ophiolites (Christensen & Lundquist 1982) are also given. A mantle consisting of a single crystal of olivine at surface conditions could produce the average splitting observed at LAK (0.45 s) with 20 to 90 km of anisotropic material, depending on its orientation. A mantle consisting of pyrolite above 220 km and piclogite below 220 km, with fully aligned olivine and pyroxenes (Estey & Douglas 1986) would require 30 to 210 km of anisotropy to produce the observed splitting. A more reasonable estimate incorporating distribution functions of crystal alignment in pyrolite would reduce the anisotropy by about half (Christensen & Lundquist 1982), and double the required thickness of the anisotropic layer to 60 to 420 km.

A vertical orientation of the olivine [100] axis is unlikely for a reasonable mantle model because the shear-wave splitting observed for some earthquakes (0.9 s) could not be produced within the upper 400 km of the mantle, and anisotropy has not yet been observed elsewhere below 400 km. If olivine [100] and orthopyroxene [001] axes are aligned with the direction of flow as inferred for ophiolites (Christensen 1984), then a horizontal [100] axis implies horizontal flow in the upper mantle beneath LAK. The thickness of the anisotropic portion of the upper mantle must be at least 60 to 70 km (Table 3). The oldest rocks reported on the Lau Ridge are 14 Myr (Woodhall 1984), while maximum magnetic-lineations suggest an age of 6 Myr for the Lau Basin (Weissel 1977). Taking 14 Myr as the age of the lithosphere under LAK, the lithosphere should be about 30 to 35 km thick (Watts, Bodine & Steckler 1980). Thus, the anisotropy must extend below the base of the lithosphere. If we discount observations of anisotropy in the lithosphere, on the other hand, then the asthenosphere alone could account for the observed splitting.

The choice between vertical [010] and [001] olivine axes cannot be made with the data presented here. In either case, though, [100] is the fast polarization direction for vertically propagating *S*-waves in olivine (Verma 1960) or peridotite (Christensen & Lundquist 1982) and must correspond to the ESE fast direction inferred from splitting.

Tectonic interpretation of shear-wave splitting

The orientation of fast *S*-wave components observed at LAK (Fig. 6a) and the implied olivine [100] orientation is superimposed on a map of magnetic lineations in Fig. 8 (Malahoff, Feden & Fleming 1982b). As discussed above, the [100] axis of olivine is aligned with the inferred direction of flow (e.g. Christensen 1984). The fast direction is approximately perpendicular to the magnetic lineations in the Lau Basin and the northeastern South

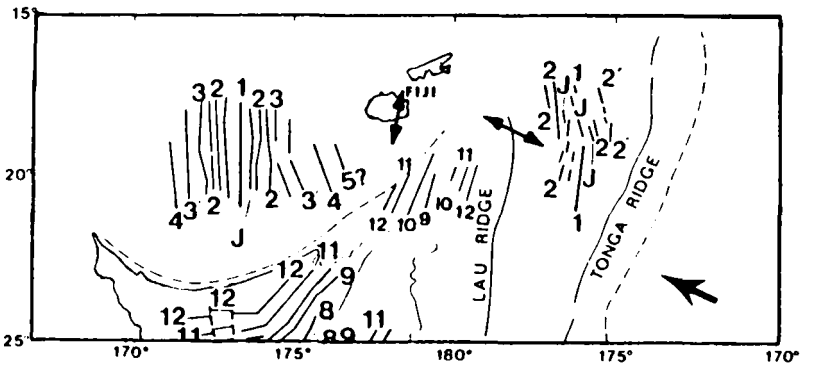

Figure 8. Magnetic lineation trends in the Fiji–Tonga area (after Malahoff *et al.* 1982b). Double arrows show fast velocity directions from Fig. 6 plotted at stations LAK and SVA. Single arrow shows direction of plate convergence (from Minster & Jordan 1978).

Fiji Basin. Thus, the direction of flow deduced from shear-wave splitting is nearly parallel to the direction of extension of these basins and to the direction of convergence between the Pacific and Australia–India plates (Minster & Jordan 1978). The fast P_n direction measured 1000 km east of the Tonga Trench is NNE (Shearer & Orcutt 1985). However, the fast P_n direction reflects the direction of flow at the ridge at the time of formation and is not related to subduction or back-arc processes.

The orientation of the fast *S*-wave component at SVA (Fig. 6b) is less well defined than at LAK, but is approximately parallel to the magnetic lineations (Fig. 8). The average 0.65 s splitting observed at SVA also requires anisotropy in the asthenosphere by the same arguments presented above for LAK. Viti Levu is thought to be an extension of the Lau Ridge (Gill & Gorton 1973) which has been rotated 90° counter-clockwise into its current position (Malahoff *et al.* 1982a). It is not surprising, then, that anisotropy in the underlying mantle does not reflect the same flow orientation that produced the anisotropy under the Lau Ridge. If the lithosphere and asthenosphere under Viti Levu have undergone the same rotation as the crust, then the orientation of the fast *S*-wave direction may correspond to the former flow direction which has been rotated by 90°. Alternatively, the shear stress that produced the rotation may have generated a new mineral alignment.

If anisotropy in the upper-mantle wedge behind the Tonga subduction zone is produced by large-scale tectonic processes as described above, then local variations in the direction and magnitude of shear-wave splitting would not be expected. Measurement errors are estimated to be ±25° and ±0.2 s, and result primarily from broad correlation peaks and *P*-coda noise. The variation in the observed splitting vectors exceeds these estimates (Figs 6 and 7). Several factors may contribute to the variation in shear-wave splitting. One possibility is that there is not a simple horizontal flow structure in the mantle underlying the Lau Ridge and Fiji Platform. Extension of the Lau Basin may have ocurred by complex dike intrusion or point volcanism over a broad region as suggested by the diffuse magnetic anomaly pattern (Lawver & Hawkins 1978). This type of spreading mechanism has been inferred from the internal structure of some ophiolite complexes (Nicolas & Violette 1982), and could produce variation in flow alignment of mantle minerals on a scale of tens of kilometres. This in turn would cause local variation in the orientation of anisotropic symmetry axes. Another possible cause of the variation in shear-wave splitting is lateral heterogeneity near either the source or receiver. Lateral heterogeneity could produce deviations in the shear-wave polarization of up to 10° from that expected for a homogeneous earth (Cormier 1984), but

this alone could not account for the observed variation of fast *S*-wave direction. Lateral heterogeneity can also result in multipathing which can modify the *S* arrivals by phase interference. Multipathing probably produces second phases for some deep earthquakes (Bowman 1985), but these can usually be distinguished from shear-wave splitting. Scattering from complex crustal structure may be less easy to recognize and could introduce additional error in estimates of splitting. Lateral variation in mineralogy, particularly in the concentration of olivine, or in the degree of crystal alignment would contribute to the variation in the magnitude of the observed shear-wave splitting.

Conclusions

Shear waves of 22 deep earthquakes recorded at station LAK on the Lau Ridge are split by 0.45 ± 0.25 s with the fast *S*-wave component generally orientated ESE. This shear-wave splitting is probably caused by seismic velocity anisotropy in the mantle between the Moho and depths of at least 60 to 70 km. Anisotropy in the asthenosphere is required to produce the observed splitting. The fast *S*-wave direction corresponds to an axis of symmetry of the anisotropic mantle and, by analogy to interpretations of ophiolite petrofabrics, corresponds to the direction of flow in the upper mantle. The inferred flow direction is nearly parallel to the direction of spreading implied by the orientation of magnetic anomalies in the South Fiji and Lau Basins. Shear waves of three earthquakes recorded at LAK have linear polarizations aligned with the fast velocity direction suggesting that the source polarizations were close to an axis of symmetry for these events. Variations in the orientations of fast shear-waves observed at LAK may be the result of a complex flow pattern during spreading of the Lau Basin by dike intrusion, or due to scatter from lateral heterogeneities.

Shear waves of eight deep earthquakes recorded at SVA on Viti Levu are split by 0.65 ± 0.29 with a north–northeast preferred fast *S*-wave direction. The orientation may reflect the 90° counter-clockwise rotation of Viti Levu in the past 7 Myr. The scatter in the orientations at SVA may reflect the complex tectonic history of the Fiji platform.

Acknowledgments

The authors thank the Mineral Resources Department of Fiji and the teachers at the Ratu Finau School of Lakeba for cooperation with data collection. Special thanks to I. B. Everingham, L. Vuetibau and I. Baleilomaloma. Critical reviews by S. Billington, L. Estey, M. Hamburger, I. Kawasaki and C. Kisslinger were very helpful. This work was supported by NSF grant EAR-8212731.

References

Agterberg, F. P., 1974. *Developments in Geomathematics*, Elsevier, Amsterdam.

Anderson, D. L., 1979. The upper mantle transition region: Eclogite? *Geophys. Res. Lett.*, **6**, 443–436.

Anderson, D. L., 1984. The earth as a planet: Paradigms and paradoxes, *Science*, **223**, 347–355.

Ando, M., 1984. *ScS* polarization anisotropy around the Pacific Ocean, *J. Phys. Earth*, **32**, 179–196.

Ando, M., Ishikawa, Y. & Yamazaki, F., 1983. Shear wave polarization anisotropy in the upper mantle beneath Honshu, Japan, *J. geophys. Res.*, **88**, 5850–5864.

Billington, S., 1980. The morphology and tectonics of the subducted lithosphere in the Tonga–Fiji–Kermadec region from seismicity and focal mechanism solutions, *PhD thesis*, Cornell University.

Bowman, J. R., 1985. Anisotropy and attenuation in the upper mantle in the Fiji and Tonga region, *PhD thesis*, University of Colorado.

Christensen, N. I., 1984. The magnitude, symmetry and origin of upper mantle anisotropy based on fabric analyses of ultramafic tectonites, *Geophys. J. R. astr. Soc.*, **76**, 89–111.

Christensen, N. I. & Lundquist, S. M., 1982. Pyroxene orientation within the upper mantle, *Bull. geol. Soc. Am.*, **93**, 279–288.

Christensen, N. I. & Salisbury, M. H., 1979. Seismic anisotropy in the upper mantle: Evidence from the Bay of Islands ophiolite complex, *J. geophys. Res.*, **86**, 2545–2555.

Cormier, V. F., 1984. The polarization of *S*-waves in a heterogeneous isotropic earth model, *J. geophys. Res.*, **56**, 20–23.

Dziewonski, A. M. & Anderson, D. L., 1981. Preliminary reference earth model, *Phys. Earth planet. Int.*, **25**, 297–356.

Estey, L. H. & Douglas, B. J., 1986. Upper-mantle anisotropy: A preliminary model, *J. geophys. Res.*, in press.

Estey, L. H., Douglas, B. J. & Spetzler, H., 1986. A synthesis for the upper mantle: I. Anisotropy, *Rev. Geophys. Space Phys.*, submitted.

Evans, R., 1984. Effects of the free surface on shear wavetrains, *Geophys. J. R. astr. Soc.*, **76**, 165–172.

Fukao, Y., 1984. Evidence from core-reflected shear waves for anisotropy in the Earth's mantle, *Nature*, **309**, 695–698.

Forsyth, D. W., 1975. The early structural evolution of the oceanic upper mantle, *Geophys. J. R. astr. Soc.*, **43**, 103–162.

Gill, J. & Gorton, M., 1973. A proposed geological and geochemical history of eastern Melanesia, in *The Western Pacific: Island Arcs, Marginal Seas and Geochemistry*, pp. 543–566, ed. Coleman, P. J., University of W. Australia Press.

Grand, S. P. & Helmberger, D. V., 1984. Upper mantle shear structure of North America, *Geophys. J. R. astr. Soc.*, **76**, 399–438.

Hess, H., 1964. Seismic anisotropy of the uppermost mantle under oceans, *Nature*, **203**, 620–631.

Kanasewich, E. R., Alpaslan, T. & Hron, F., 1973. The importance of *S*-wave precursors in shear-wave studies, *Bull. seism. Soc. Am.*, **63**, 2167–2176.

Karig, D. E., 1970. Ridges and basins of the Tonga–Kermadec island arc system, *J. geophys. Res.*, **75**, 239–254.

Kasahara, J., Suzuki, I., Kumazawa, M. & Iida, K., 1968. Anisotropy of *S*-wave in dunite, *Zisin*, **21**, 229–236.

Kawasaki, I., 1986. Azimuthally anisotropic model of the oceanic upper mantle, *Phys. Earth planet. Int.*, **43**, 1–21.

Keith, C. M. & Crampin, S., 1977. Seismic body waves in anisotropic media: synthetic seismograms, *Geophys. J. R. astr. Soc.*, **49**, 225–243.

Kroenke, L. W., Jouannic, C. & Woodward, P., 1983. *Bathymetry of the southwest Pacific: Chart 1 of the Geophysical Atlas of the Southwest Pacific*, CCOP/SOPAC.

Lawver, L. A. & Hawkins, J. W., 1978. Diffuse magnetic anomalies in marginal basins: their possible tectonic and petrological significance, *Tectonophys.*, **45**, 323–339.

Malahoff, A., Hammond, S. R., Naughton, J. J., Keeling, D. L. & Richmond, R. N., 1982a. Geophysical evidence for post-Miocene rotation of the island of Viti Levu, Fiji, and its relationship to the tectonic development of the North Fiji Basin, *Earth planet. Sci. Lett.*, **57**, 398–414.

Malahoff, A., Feden, R. H. & Fleming, H. S., 1982b. Magnetic anomalies and tectonic fabric of marginal basins north of New Zealand, *J. geophys. Res.*, **87**, 4109–4125.

Mendiguren, J. A., 1969. Study of focal mechanism of deep earthquakes in Argentina using non-linear particle motion of *S* waves, *Bull. seism. Soc. Am.*, **59**, 1449–1473.

Minster, J. B. & Jordan, T. H., 1978. Present-day plate motions, *J. geophys. Res.*, **83**, 5331–5354.

Musgrave, M. J. P., 1970. *Crystal Acoustics*, Holden-Day, San Francisco.

Nicolas, A. & Violette, J. F., 1982. Mantle flow at oceanic spreading centers: Models derived from ophiolites, *Tectonophys.*, **81**, 319–339.

Nuttli, O., 1961. The effect of the earth's surface on the *S*-wave particle motion, *Bull seism. Soc. Am.*, **51**, 237–246.

Oliver, J. & Isacks, B., 1967. Deep earthquake zones, anomalous structures in the upper mantle, and the lithosphere, *J. geophys. Res.*, **72**, 4259–4275.

Pennington, W. D. & Isacks, B. L., 1979. Analysis of short-period waveforms of *P* phases from deep-focus earthquakes beneath the Fiji islands, *Geophys. J. R. astr. Soc.*, **56**, 19–40.

Peselnick, L. & Nicolas, A., 1978. Seismic anisotropy in an ophiolite peridotite: Application to oceanic upper mantle, *J. geophys. Res.*, **83**, 1227–1235.

Pincus, H. J., 1956. Some vector and arithmetic operations on two-dimensional orientation variates, with applications to geologic data, *J. Geol.*, **64**, 533–557.

Raitt, R. W., Shor, G. G., Morris, G. B. & Kirk, H. K., 1971. Mantle anisotropy in the Pacific Ocean, *Tectonophys.*, **12**, 173–186.

Reagan, J. & Anderson, D. L., 1984. Anisotropic models of the upper mantle, *Phys. Earth planet. Int.*, **35**, 227–263.

Schule, J. W. & Knopoff, L., 1977. Shear-wave polarization anisotropy in the Pacific Basin, *Geophys. J. R. astr. Soc.*, **49**, 145–165.

Shearer, P. & Orcutt, J., 1985. Anisotropy in the oceanic lithosphere – theory and observations from the Ngendei seismic refraction experiment in the south-west Pacific, *Geophys. J. R. astr. Soc.*, **80**, 493–526.

Shimamura, H., 1984. Anisotropy in the oceanic lithosphere of the northwestern Pacific Basin, *Geophys. J. R. astr. Soc.*, **76**, 253–260.

Sykes, L. R., Isacks, B. L. & Oliver, J., 1969. Spatial distribution of deep and shallow earthquakes of small magnitudes in the Fiji–Tonga region, *Bull. seism. Soc. Am.*, **59**, 1093–1113.

Tanimoto, T. & Anderson, D. L., 1984. Mapping convection in the mantle, *Geophys. Res. Lett.*, **11**, 287–290.

Verma, R. K., 1960. Elasticity of some high-density crystals, *J. geophys. Res.*, **65**, 757–766.

Watts, A. B., Bodine, J. H. & Steckler, M. S., 1980. Observation of flexure and the state of stress in the oceanic lithosphere, *J. geophys. Res.*, **85**, 6369–6376.

Weissel, J. K., 1977. Evolution of the Lau Basin by growth of small plates, in *Island Arcs, Deep Sea Trenches and Back Arc Basins, Maurice Ewing Ser., Vol. 1*, pp. 429–436, ed. Pitman, W. D., A.G.U., Washington D.C.

Woodhall, D., 1984. The geology of the Lau Ridge, in *Geologic and resource investigations of the southern Tonga platform and nearby regions: Initial results of cruise CCOP/SOPAC L5-82 and supporting investigations*, ed. Vallier, T. L.